THE JOURNAL OF PHYSICAL CHEMISTRY B

Article

pubs.acs.org/JPCB

IR, Raman, and NMR Studies of the Short-Range Structures of $0.5Na_2S + 0.5[xGeS_2 + (1-x)PS_{5/2}]$ Mixed Glass-Former Glasses

Christian Bischoff,† Katherine Schuller, Nathan Dunlap, and Steve W. Martin†

Department of Materials Science and Engineering, Iowa State University of Science & Technology, Ames, Iowa 50011, United States

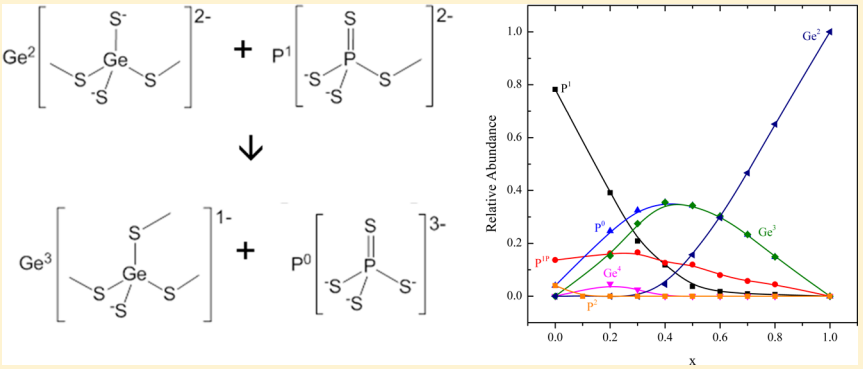

ABSTRACT: A nonlinear and nonadditive composition-dependent change of the ionic conductivity in mixed glass-former (MGF) glasses when one glass former, such as $PS_{5/2}$, is replaced by a second glass former, such as GeS_2, at constant alkali modifier concentrations, such as Na_2S, is known as the mixed glass-former effect (MGFE). Alkali ion conducting glasses are of particular interest for use as solid electrolytes in alkali-based all-solid-state batteries because sulfide amorphous materials have significantly higher alkali ion conductivities than their oxide glass counterparts. In this study of the ternary MGF system $Na_2S + GeS_2 + PS_{5/2}$, we report the careful structural characterization of these glasses using a combination of vibrational, infrared (IR), Raman, and nuclear magnetic resonance (NMR) spectroscopies. Our measurements of the $0.5Na_2S + 0.5[xGeS_2 + (1-x)PS_{5/2}]$ MGF system show that this glass system exhibits a strongly negative MGFE and non-Arrhenius ionic conductivities. While this negative MGFE in the Na^+ ion conductivity makes these glasses less attractive for use in solid-state Na batteries, the structural origin of this effect is important to better understand the mechanisms of ion conduction in the glassy state. For these reasons, we have examined the structures of ternary $0.5Na_2S + 0.5[xGeS_2 + (1-x)PS_{5/2}]$ glasses using Raman, IR, and ^{31}P MAS NMR spectroscopies. In these studies, it is found that the substitution of $PS_{5/2}$ by GeS_2, that is, increasing x, leads to unequal sharing of the Na^+ in these glasses. Thus, in all MGF compositions, phosphorus groups are associated with a disproportionately larger fraction, $f_{Na(P)} > 0.5(1-x)$, of the Na^+ ions while the germanium groups are found to be Na^+-deficient relative to the total amount of Na^+ present in the glass, that is, $f_{Na(Ge)} < 0.5x$. From the spectroscopic study of these glasses, a short-range order (SRO) structural model is developed for these glasses and is based on the germanium and phosphorus SRO groups in these glasses as a first step in understanding the unique negative MGFE and non-Arrhenius behavior in the Na^+ ion conductivity in these glasses.

1. INTRODUCTION

Reliable, safe, low-cost, and large-capacity energy storage systems are required to enable renewable energy systems such as wind turbines and solar cells to make greater contributions to the global electrical energy grid. Global conversion and consumption of energy is currently ~15 TW and is expected to double by 2050.[1,2] The typical electrical power profile of renewable energy sources, chiefly solar and wind, are cyclic in nature,[1,3−5] and as such, energy storage systems such as batteries are critically needed to accommodate the mismatches between renewable energy harvesting and demand. This rapidly growing demand requires the development of new energy storage technologies.

Currently, rechargeable lithium ion batteries depend on liquid electrolytes that can foster lithium dendrite growth, leading to severe safety concerns.[4,6] The design of new solid electrolytes with sufficiently high alkali ion conductivities, at least 10^{-3} S/cm at 25 °C, may offer a solution to this safety problem. Alkali ion conducting glasses may be able to meet these challenging design constraints. Indeed, these glasses are of particular interest because they can improve chemical durability and, in some cases, improve ionic conductivity.[7−10]

A rare coincidence of high ionic conductivity with improved physical and electrochemical properties of glassy electrolytes can be achieved by mixing two glass-former cations, such as Ge^{4+} and P^{5+}, at constant fraction of the mobile cation, such as Li^+ and Na^+, known as the mixed glass-former effect (MGFE).[9,11−14] Optimized mixed glass-former (MGF) glassy

Received: November 11, 2013
Revised: January 17, 2014
Published: January 21, 2014

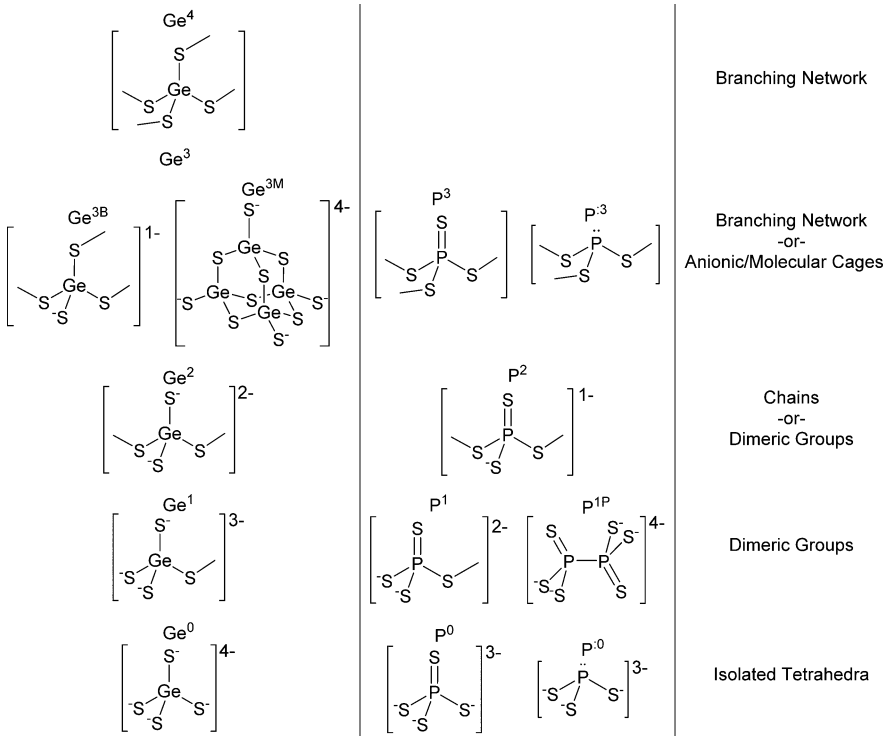

Figure 1. Local germanium environments (left), local phosphorus environments (middle), and corresponding intermediate-range order (right).

solid electrolytes may be excellent candidates for next-generation solid-state electrolytes. For these reasons, we have begun an in-depth study of the MGFE in oxide and sulfide glasses. Currently, the structures and properties of sodium-modified MGF systems that include B_2O_3, SiO_2, P_2O_5, SiS_2, GeS_2, and P_2S_5 glass formers are being characterized in an effort to better understand and exploit the MGFE to enable optimized solid electrolytes for next-generation alkali-ion-based batteries. The MGFE studies of oxide glasses in our group have confirmed findings in the literature that mixing an alkali borate glass with an alkali phosphate glass produces a strong and positive MGFE[15−18] while improving our knowledge of the structural origins of the MGFE. While more difficult to prepare and study, sulfide glasses are attractive for study due to their higher ionic conductivities relative to oxide glasses typically being on the order of 10^{-5} to 10^{-2} $(\Omega\ \mathrm{cm})^{-1}$ for the former[12,19−22] compared to 10^{-9}−$10^{-6}(\Omega\ \mathrm{cm})^{-1}$ for the latter.[8,23−26]

As described above, alkali thiophosphate glasses have high alkali, especially lithium, ion conductivities[27−29] and for these reasons have been used extensively in solid-state lithium batteries.[30−32] Furthermore, phosphate glasses are attractive for structure−property correlation studies because ^{31}P is a nearly 100% atomic abundant spin-1/2 nucleus, allowing the phosphorus structures to be probed with NMR techniques.[33−38] These reasons have motivated our selection of $PS_{5/2}$ as one glass former for study of the MGFE in sulfide glasses. Note, we use the reduced $PS_{5/2}$ formula unit here so that compositionally, the ternary when used with GeS_2 substitutes one glass former, P, for another Ge. GeS_2 was chosen as a second glass former because it has a large glass-forming range for the yNa$_2$S + $(1-y)$GeS$_2$ glasses, which will be described in more detail below, and the short-range order (SRO) structures in these glasses can be probed with vibrational spectroscopy. Further, because these two binary glasses have received only modest investigation and as such are only lightly reported in the literature,[39−41] we spend some effort here to describe the structures of the binary yNa$_2$S + $(1-y)$GeS$_2$ and yNa$_2$S + $(1-y)$PS$_{5/2}$ glasses as a basis for better understanding the structures of the ternary glasses.

Only a limited number of structural studies of the yNa$_2$S + $(1-y)$GeS$_2$, yNa$_2$S + $(1-y)$PS$_{5/2}$, and yNa$_2$S + $(1-y)[x\mathrm{GeS}_2$ + $(1-x)\mathrm{PS}_{5/2}]$ glasses exist in the literature. Ribes et al.[42] and Maier and Van Wazer[43] report on glass-forming composition ranges in the yNa$_2$S + $(1-y)$PS$_{5/2}$ system. Our recent structural study of the binary yNa$_2$S + $(1-y)$PS$_{5/2}$ glasses, based upon Raman, IR, and NMR spectra, reveals some interesting structural information about these glasses.[44] First, the $0.5\mathrm{Na}_2\mathrm{S}$ + $0.5\mathrm{P}_2\mathrm{S}_5$, NaPS_3 metathiophosphate composition shows evidence of edge-sharing $\mathrm{NaSPS}_{2/2}\mathrm{S}$ tetrahedra. Second, S−S bonds seem to be rather stable in these glasses, and this leads to the formation of minority phosphorus structures P^{1P} (see Figure 1), which have P−P homoatomic bonds formed by the elimination of the bridging sulfur (BS) between the two P atoms in this unit and possibly $P^{:0}$ units, which have lost the terminal and nominally doubly bonded sulfur (see Figure 1), where the $P^{:}$ means that there is a lone pair of electrons and the $P^{:0}$ means that the P unit has zero BS bonds.

The P^{1P} structural group forms when the BS, P−S−P, from $P_2S_7^{4-}$ anions is liberated, leaving a P−P bond. If the P^0 group, which is the completely depolymerized PS_4^{3-} tetrahedral anion, loses its doubly bound sulfur, a lone pair of electrons remains on the phosphorus cation, forming the trigonal pyramidal $P^{:0}$ group.

Low-alkali glasses in the yNa$_2$S + $(1-y)$GeS$_2$ system, $y \leq 0.4$, were studied by Zhou et al.,[45] while Ribes et al.[42] and Barrau et al.[41] reported a wider composition range, $0.0 \leq y \leq 0.6$. The SRO structures of the various glasses in this system exhibit GeS_4 tetrahedra, all with varying numbers of nonbridging sulfurs (NBSs), Ge−S$^-$ Na$^+$; see Figure 1. Addition of the ionic

dx.doi.org/10.1021/jp4111053 | J. Phys. Chem. B 2014, 118, 1943−1953

and basic Na_2S leads to depolymerization of the $GeS_{4/2}$ tetrahedra to form NBS units, from 0 for $y = 0$ up to 4 at $y = 0.66$. Consistent with the work of Ribes[39] and Barrau,[41] the glass-forming range in this binary glass system ends before the totally depolymerized Na_4GeS_4, Ge^0 group, is reached. Representations of the five SRO germanium structures are shown in Figure 1. Studies of the structures and properties of lithium thiogermanate glasses, $yLi_2S + (1-y)GeS_2$, have also been reported in the literature,[9,12,13] and the SRO structures of these glasses are very similar to those found for their sodium analogues, but the glass-forming range of $0.35 \leq y \leq 0.6$ is somewhat narrower (on the GeS_2-rich end) than that in the sodium-modified glasses. Phase separation and crystallization occur at low Li_2S content compositions near $y = 0$ or pure GeS_2.[9]

In contrast to the number of studies of the binary $Na_2S + GeS_2$ glasses, very little is known of the structure and properties of ternary MGF $yNa_2S + (1-y)[xGeS_2 + (1-x)PS_{5/2}]$ glasses. Blachnik and Rabe[46] have reported the partial phase diagram along the compositional line $Na_4Ge_4S_{10}$–P_4S_{10}. They found that the compound $Na_4Ge_4S_{10}$ is isostructural with P_4S_{10}, which is a molecular solid with an adamantine-type structure. For the binary mixtures of $Na_4Ge_4S_{10}$ and P_4S_{10}, Blachnik and Rabe found that the $Na_4Ge_4S_{10}$ groups reacted with the P_4S_{10} molecules to form $NaPS_3$ chain structures and Na_3PS_4 groups that have isolated PS_4^{3-} tetrahedral anions surrounded by three Na^+ ions. This disproportionate sharing of Na^+ ions toward the phosphorus groups leads to the removal of Na^+ from the Ge structures and to subsequent polymerization of Ge–S structures that have larger numbers of BS units and fewer NBSs and as a result yielded solid glassy solutions that were assumed to be comprised of GeS_2, $Na_4Ge_4S_{10}$, $NaPS_3$, Na_3PS_4, and P_4S_{10}.[46] We will report below a similar disproportionate sharing of the Na^+ between Ge^{4+} and P^{5+} in the larger compositional study that we have begun here. While these partial studies of the ternary $yNa_2S + (1-y)[xGeS_2 + (1-x)PS_{5/2}]$ glasses have been reported in the literature, we have begun a more complete study of these glasses to better understand the structures of the $yNa_2S + (1-y)[xGeS_2 + (1-x)PS_{5/2}]$ glasses, which as described above are not well-reported in the open literature. In the process of this study, we have also examined the structures of the binary $yNa_2S + (1-y)GeS_2$ and the $yNa_2S + (1-y)PS_{5/2}$ glasses. This study has been motivated by our observation (to be reported in a separate publication) of a negative MGFE in the Na^+ ion conductivity in these glasses.

We have used Raman and IR vibrational spectroscopies to examine the structures of the binary $yNa_2S + (1-y)GeS_2$ glasses and ^{31}P magic angle spinning nuclear magnetic resonance (MAS NMR) to examine the binary $yNa_2S + (1-y)PS_{5/2}$ glasses. Results from these studies were then used to interpret the Raman, IR, and ^{31}P MAS NMR spectra of the ternary $0.5Na_2S + 0.5[xGeS_2 + (1-x)PS_{5/2}]$ glasses.

2. EXPERIMENTAL METHODS

2.1. Sample Preparation. All syntheses were carried out in a high-purity N_2 glovebox, where O_2 and H_2O levels are consistently below 10 ppm and often well below 1 ppm. Because high-purity Na_2S is not commercially available, it was synthesized in our laboratory by the thermal decomposition of $Na_2S{\cdot}9H_2O$. Appropriate weighed amounts of the $Na_2S{\cdot}9H_2O$ were placed in a vitreous carbon crucible that was then placed inside of a hermetically sealed stainless steel reaction chamber. This reaction chamber was then placed in a vertical crucible furnace so that the sample was within the heated zone of the furnace and part of the reaction chamber extended outside of the furnace. The reaction chamber was then sealed with a water-cooled stainless-steel top that uses a rubber O-ring to hermetically seal the top to the reaction chamber and connected to a vacuum pump. A liquid-nitrogen-cooled trap was connected between the reaction chamber and the vacuum pump to trap the volatized water before it entered the vacuum pump. The hydrated crystalline material was then slowly heated under vacuum, ~30 mbar, up to 150 °C over a period of at least 2 h, after which the temperature was slowly increased to 650 °C at ~1 °C/min, held for approximately 20 h, and then slowly cooled to room temperature. The reaction chamber was then disconnected from the vacuum line and while still under vacuum and containing the now dehydrated Na_2S was transferred to the glovebox, vented, and unloaded. IR spectroscopy and X-ray diffraction (XRD) were used to confirm the absence of contaminate oxides and the phase purity of the Na_2S, respectively, of the material.

High-purity glassy GeS_2 was also prepared in our laboratory by reacting stoichiometric amounts of germanium powder and sulfur in an evacuated silica ampule at 900 °C for approximately 16 h. The glass ampule was air quenched to room temperature, and glassy GeS_2 was obtained. Phosphorus pentasulfide (P_2S_5) is commercially available and was used as received (99.9% Sigma-Aldrich).

Glass batches of 3–4 g were made by combining appropriate amounts of the starting material powders to create the $yNa_2S + (1-y)GeS_2$ and $yNa_2S + (1-y)PS_{5/2}$ glasses, where the thiophosphate glass was milled in a planetary mill to minimize evaporation of $PS_{5/2}$ during melting by a prereaction of the Na_2S and $PS_{5/2}$. The ternary $yNa_2S + (1-y)[xGeS_2 + (1-x)PS_{5/2}]$ glasses were prepared by mixing the appropriate amounts of the binary $yNa_2S + (1-y)GeS_2$ and $yNa_2S + (1-y)PS_{5/2}$ glasses for the series $y = 0.5$. These mixtures were then melted in covered vitreous carbon crucibles inside of a mullite muffle tube furnace at 550–800 °C, where lower temperatures were used for the thiophosphate-rich glasses and the higher temperatures were used for the thiogermanate-rich glasses, hermetically connected to the side of the glovebox for 3–5 min. The samples were then removed from the furnace and allowed to cool inside of the crucible. Mass losses were recorded and in all cases found to be less than 2 wt %, and the glasses were then remelted at the same temperature for an additional 3 min and quenched to room temperature between brass plates (>10^4 °C/s). All samples were transparent and showed no visual signs of crystallization and/or phase separation. XRD was performed on representative samples to confirm the absence of any partial crystallinity in the quenched glasses. In an effort to better assign SRO structures, as will be described below, glass samples of some of the compositions were purposefully crystallized by heating the samples to a temperature just above the onset of the first crystallization exotherm, identified by differential scanning calorimetry (DSC), and held for several hours.

2.2. Raman Spectroscopy. A Renishaw inVia Raman spectrometer employing a 488 nm Ar^+ laser was used to collect the Raman spectra from 100 to 3200 cm^{-1} using a 20× objective and 10 mW of power. For each sample, three scans were co-added to improve the signal-to-noise ratio. An internal silicon reference was used to calibrate the instrument, where the very sharp silicon mode at 520 cm^{-1} was reproducible to within ±1 cm^{-1}. Small glass pieces were placed into a small plastic sample holder and covered with transparent tape to

dx.doi.org/10.1021/jp4111053 | J. Phys. Chem. B 2014, 118, 1943–1953

prevent exposure to air. The microscope was focused through the tape onto the surface of the glass pieces. The reproducibility of the Raman spectra while focusing on multiple spots across the samples was further evidence of sample homogeneity.

2.3. IR Spectroscopy. Mid-IR spectra were collected using a Bruker IFS 66 v/s vacuum infrared spectrometer in the range of 4000−400 cm^{-1} using a KBr beamsplitter. The IR spectra were obtained using 32 scans at 4 cm^{-1} resolution. Far-IR spectra were collected in the same manner from 600 to 130 cm^{-1} using a germanium-coated Mylar beamsplitter. To assist in handling and loading these air-sensitive samples, the spectrometer was equipped with a small glovebox ante-chamber that was purged with N_2 gas. Samples were held in this small ante-chamber until loaded into the spectrometer where the spectra were taken under vacuum. The IR spectra of the samples were taken by diluting the finely ground glass powder to approximately 2% in finely ground and carefully dried CsI and then pressed into small pellets.

2.4. Magic Angle Spinning Nuclear Magnetic Resonance (MAS NMR). Single-pulse ^{31}P NMR studies were performed at 242.9 MHz on a Bruker Avance II 600 spectrometer, equipped with a multinuclear MAS probe from Bruker. Finely ground samples loaded inside of the glovebox were spun within capped zirconia 2.5 mm rotors at 22−25 kHz, depending on the sample, unless otherwise noted. Spectra were collected using 128−256 scans, a 2 μs, 72° pulse length, and a 100−300 s recycle delay. Chemical shifts were externally referenced to 85% (aq) H_3PO_4.

3. RESULTS AND DISCUSSION

3.1. Glass-Forming Ranges. Due to the glass-forming character of GeS_2 and the high quench rate, estimated to be $>10^4$ °C/s, stoichiometric glasses were prepared in the $y$$Na_2S$ + $(1-y)$$GeS_2$ glasses for y = 0, 0.33, 0.5, 0.6, and 0.67. The $y$$Na_2S$ + $(1-y)$$PS_{5/2}$ glasses are strongly glass-forming for $0.33 \leq y < 0.6$. Interestingly, a small glass-forming window also exists near y = 0.65. A partial reason for this will be seen below to arise from the loss of sulfur from phosphorus groups in the melt. From the Raman spectra, it can be suggested that this "free sulfur" is retained in the melt and forms S_x groups and Na_2S_x polysulphides. The strong glass-forming character of the $0.5Na_2S$ + $0.5GeS_2$ and $0.5Na_2S$ + $0.5PS_{5/2}$ glasses was maintained in the ternary $0.5Na_2S$ + $0.5[xGeS_2 + (1-x)PS_{5/2}]$ glass system with the exception of the x = 0.9 glass. The non-glass-forming character of the x = 0.9 glass is not understood at this time.

3.2. Sodium Thiophosphate Glasses, yNa_2S + $(1-y)PS_{5/2}$. The vibrational spectra of the sodium thiophosphate glasses were previously studied and reported on by the authors, and a structural model was developed for these glasses.[44] To better characterize and quantify the P^n speciation in these glasses, ^{31}P MAS NMR spectra were collected and deconvoluted and fit to Gaussian peaks. In our first studies of these glasses, the ^{31}P MAS NMR spectra were collected using 4 mm rotors with a spinning rate of 12 kHz. From these studies, it became apparent that the spinning sidebands overlapped the isotropic chemical shifts of the various P^n species in these glasses. For this reason, new spectra were collected at a higher spinning rate of 22 kHz using 2.5 mm rotors, Figure 2. Surprisingly, the spectra for the y = 0.33 glass at 12 and 22 kHz look strikingly similar. Even at the higher spinning speeds, it appears that additional phosphorus environments are disguised by spinning sidebands. For these reasons, the ^{31}P MAS NMR spectra must be obtained from samples spun at even higher speeds to completely and effectively differentiate between the various P^n species.[47]

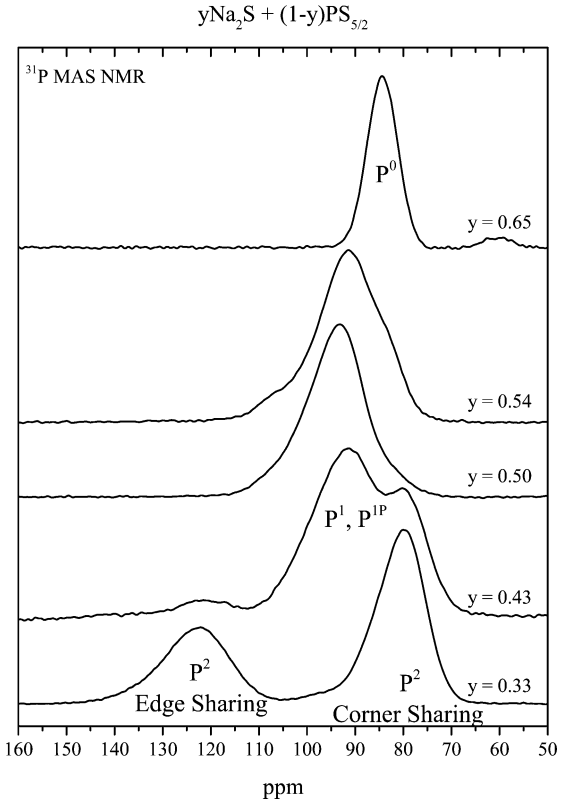

Figure 2. Composition dependence of the chemical shift of the primary peaks in ^{31}P MAS NMR spectra of the $y$$Na_2S$ + $(1-y)$$PS_{5/2}$ glasses.

With these concerns in mind, the ^{31}P MAS NMR spectrum of the y = 0.33 glass, Figure 3, exhibits two strong resonances at

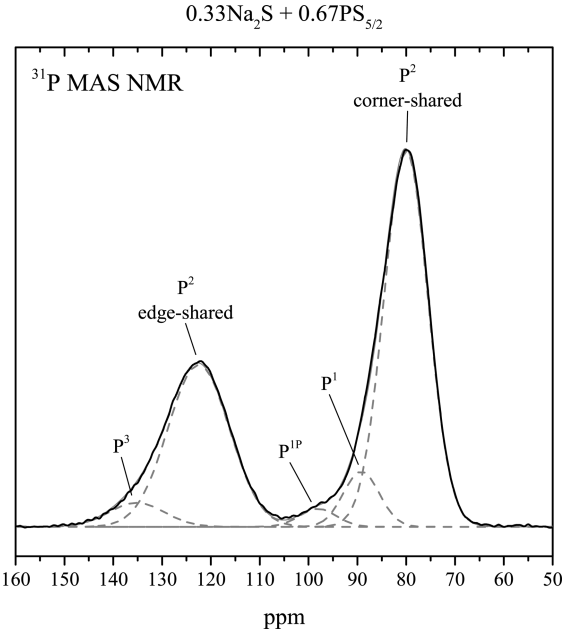

Figure 3. Example of the fitting of the ^{31}P MAS NMR spectra of the $0.33Na_2S$ + $0.67PS_{5/2}$ glass.

dx.doi.org/10.1021/jp4111053 | J. Phys. Chem. B 2014, 118, 1943−1953

82 and 125 ppm, respectively, versus 85% aq H_3PO_4. Larink et al.[47] attribute the 82 ppm resonance to the "normal" corner-shared P^2 group due to the presence of a *J*-coupling triplet and the 125 ppm resonance to P^3 groups due to a *J*-coupling quartet. Homonuclear 2D *J*-resolved spectra can help in P^n assignment, where a *z*-filtered spin−echo pulse sequence is used to collect the spectra and the P^n species can be distinguished by $^2J_{P-P}$ multiplet analysis in the indirect *J*-resolved dimension.[47−49] The multiplicity, or number of peaks, follows an $n + 1$ pattern for spin-1/2 nuclei, where n is the number of neighboring nuclei. Interestingly, the vibrational Raman and IR spectra of the $y = 0.33$ glass, shown in Figure 4

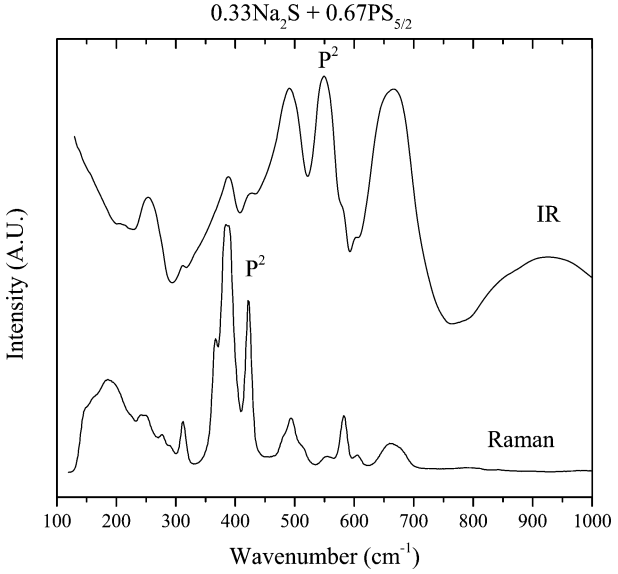

Figure 4. Raman (lower) and IR (upper) spectra of the binary $0.33Na_2S + 0.67PS_{5/2}$ glass.

and previously reported by us,[44] exhibit an intense Raman band at 422 cm^{-1} and an intense IR band at 550 cm^{-1}, both of which are evidence of significant quantities of edge-shared P^2 groups.[44,50−52] This may imply that corner- and edge-shared P^2 groups are indistinguishable by ^{31}P NMR, or it is also possible that Larink et al.[47] incorrectly attributed the 125 ppm resonance to the P^3 group. If we consider the edge-shared P^2 group, which has a P_2S_2 ring, both phosphorus atoms are coupled to only one other phosphorus, which would lead to a *J*-coupling doublet. If these two phosphorus atoms in an edge-shared P^2 group are strongly coupled, an AB quartet is expected. Under these circumstances, the 125 ppm resonance could be due to an edge-shared P^2 group. In order to definitively verify either assignment using NMR spectroscopy, *J*-resolved NMR spectra using various spectrometer frequencies are required because $^2J_{P-P}$ coupling is independent of the external magnetic field. Because this type of analysis is currently not available to us, we must consider other evidence.

If we consider charge balance, every P^3 or $P^{:3}$ structure must be balanced by a P^1 or P^{1P} structure to maintain the 1:1 ratio of Na^+ to phosphorus expected for the $y = 0.33$ glass. If the 125 ppm resonance was entirely due to P^3 or $P^{:3}$ units, then the Na^+ to phosphorus ratio would be roughly 0.6:1, indicating a loss of Na^+ ions that is not consistent with experimental weight loss measurements. However, if we assign the 125 ppm resonance to the edge-shared P^2 group, the Na^+ to phosphorus ratio would still be 1:1, as expected for a $y = 0.33$ composition. Given the evidence of edge-shared P^2 groups in the vibrational spectra of these glasses, to be discussed below, and considering the requirement of conservation of charge and no additional weight loss upon melting, we assign the 125 ppm resonance to edge-sharing P^2 groups. Using this assignment, integration of the ^{31}P NMR peak, Figure 3, indicates that 81% of the phosphorus in the glass is in P^2 groups, and of these 29% are edge-shared and 72% are corner-shared. The balance of the phosphorus, 19%, is observed to be in P^1, P^{1P}, and P^3 SRO structures. Charge balance at this composition, $y = 0.33$, requires that the sum of the P^1, P^{1P}, and P^3 groups must be governed by the disproportionation reaction

$$2P^2 \rightarrow zP^1 + (1 - z)P^{1P} + P^3$$

The SRO structures in the $y = 0.43$ glass are made up of those found in the $y = 0.33$ and 0.5 glass samples. The intermediate $y = 0.43$ glass composition has 1.5 Na^+ per phosphorus. Nominally, this should yield a $P^1/P^{(1P)}$ to P^2 ratio of 1:1. The NMR spectrum of this composition is comprised of contributions from both P^1 and P^2 groups, with a small fraction of P^{1P} groups. The $y = 0.5$ glass has a characteristic absorption peak due to the P^1 group centered at 93 ppm in the ^{31}P NMR spectrum.[53] The P^1 groups account for about 78% of the phosphorus in the sample, 14% in P^{1P} groups (104 ppm), and 8% in P^0 or P^2 groups (83 ppm), where the percentages were determined by deconvolution and integration of the NMR spectra. The vibrational spectra[44] show little evidence of P^2 groups at this composition, indicating that the shoulder on the peak at 83 ppm is due mostly to P^0 tetrahedra. This implies that the $y = 0.5$ composition has a true composition within 1 mol %. The $y = 0.54$ glass sample has 2.33 Na^+ per phosphorus, analogous to $Li_7P_3S_{11}$[54,55] or $Ag_7P_3S_{11}$.[56] The NMR spectrum confirms the presence of P^1 and P^0, which are expected to be present at this composition, but there is also evidence of a small minority of P^{1P} groups.

Because we have found that the $y = 0.6$ composition is not glass-forming, the $y = 0.65$ glass was used to characterize *ortho*-thiophosphate, P^0, structures in the glasses. The $y = 0.65$ glass composition is roughly equivalent to $Na_3PS_4 + 0.357Na_2S$. We have proposed the possible $P^{:0}$ structure based on stoichiometry considerations and vibrational modes comparable to β-Na_2S_2.[44] ^{31}P NMR should be very sensitive to the type of change in the chemical environment associated with the formation of $P^{:0}$ groups. The NMR spectrum of the $y = 0.65$ glass has a dominant intense peak with a chemical shift at about 85 ppm consistent with P^0 groups in the analogous lithium thiophosphate system.[53] A second weak resonance is observed at 60 ppm, accounting for ∼5% of the phosphorus in the glass, which we assign to the $P^{:0}$ group. This would suggest that the $P^{:0}$ group is less shielded than the P^0 group, which is consistent with the presence of a lone pair of electrons, and the +5 valence on phosphorus is conserved, leading to a trigonal pyramidal structure rather than a trigonal planar structure with a phosphorus valence of +3.

3.3. Sodium Thiogermanate Glasses, $y$$Na_2S$ + (1−y)GeS_2. The Raman and IR spectra of the binary $y$$Na_2S$ + (1−y)GeS_2 glasses are shown in Figures 5 and 6, respectively. For ease of comparison, all vibrational spectra are scaled so that the most intense bands have the same intensity for all glass compositions. Modes above 600 cm^{-1} are due to the slight but nonetheless ever present oxide contamination in these nonoxide glasses. The Raman spectra have a mode near 330 cm^{-1} (shoulder in the IR spectra) that diminishes with

dx.doi.org/10.1021/jp4111053 | J. Phys. Chem. B 2014, 118, 1943−1953

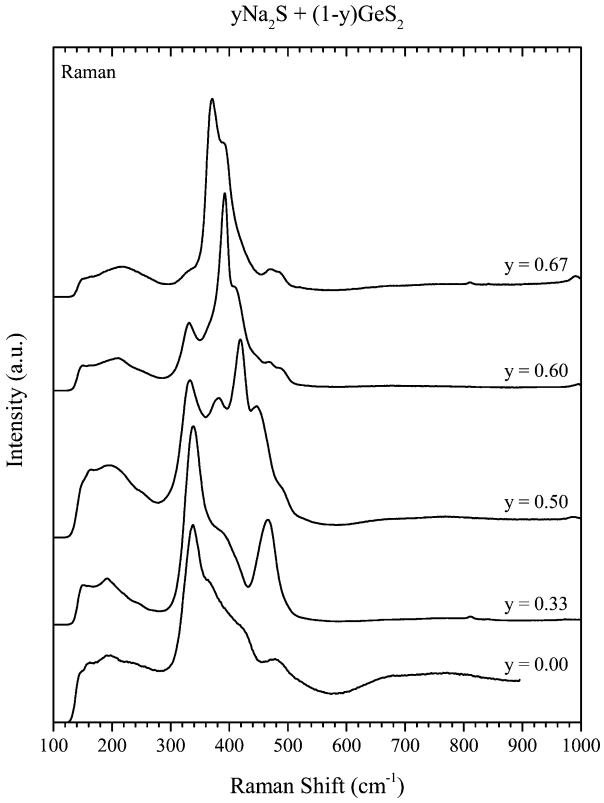

Figure 5. Composition dependence of the Raman spectra of the binary $y\mathrm{Na_2S} + (1-y)\mathrm{GeS_2}$ glasses.

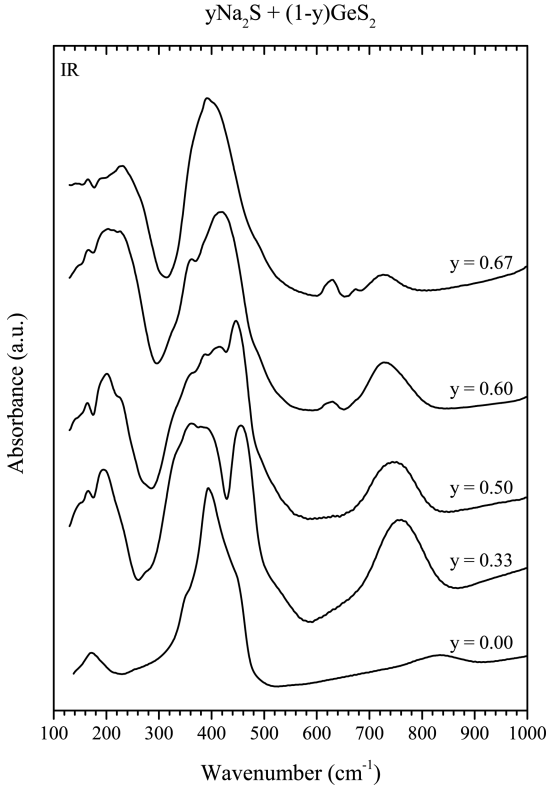

Figure 6. Composition dependence of the IR spectra of the $y\mathrm{Na_2S} + (1-y)\mathrm{GeS_2}$ glasses.

increasing Na_2S content. This spectral feature is due to BS between germanium groups, Ge−S−Ge. NBS structures give rise to a Raman mode centered at 465 cm^{-1} for the $y = 0.33$ glass, and this mode shifts to lower frequency with increasing Na_2S content, where it is ultimately centered at 371 cm^{-1} for the $y = 0.67$ glass. A similar trend is present in the IR spectra of the glasses with the NBS, giving rise to a mode at 455 cm^{-1} for the $y = 0.33$ glass that shifts to 391 cm^{-1} for the $y = 0.67$ glass.

As described above, the SRO structures of the sodium thiogermanate glasses are characterized by Ge^n tetrahedra, where n denotes the number of BSs.[41,42,57,58] The $y = 0$ glass, or pure GeS_2 glass, has Ge^4 groups that are predominantly corner-sharing, forming a three-dimensional branching network, as in β-GeS_2.[57] A minority of edge-sharing tetrahedra, as in α-GeS_2, may also be present in the glass.[57] The most intense Raman and IR bands present in Figures 5 and 6, respectively, are centered near 343 and 395 cm^{-1}. The Raman mode at 343 cm^{-1} is due to the A_1 symmetric stretching of the Ge^4 tetrahedra, and the IR mode at 395 cm^{-1} is due to the T_2 deformation of the Ge^4 tetrahedra. These results are in good agreement with literature values for GeS_2 glass and β-GeS_2.[41,57,58]

The addition of Na_2S to GeS_2, which possesses the Ge^4 structure (see Figure 1), leads to the formation of Ge^3 structures. The Ge^3 structural unit, or $Na_2S/2GeS_2$, dithiogermanate, corresponds to the $y = 0.33$ composition. Starting with the Raman bands, the most intense mode is centered at 339 cm^{-1} in Figure 5, which is assigned to symmetric stretching of the Ge^3 tetrahedron. The broad, high-frequency shoulder (~390 cm^{-1}) is attributed to BS Ge−S−Ge. The mode centered at 465 cm^{-1} is due to stretching of terminal NBS. Turning to the IR spectrum in Figure 6, a band centered at 456 cm^{-1} is due to stretching of terminal sulfur. A very broad feature is centered near 370 cm^{-1}, which appears to be a mixture of multiple modes centered near 330, 360, 380, and 390 cm^{-1}, respectively, that are not easily differentiated. Comparison with crystallized samples of the $y = 0.33$ composition is required to better identify the structural groups present in the $0.33\mathrm{Na_2S} + 0.67\mathrm{GeS_2}$ glass.

Figure 7 shows the Raman and IR spectra of the polycrystalline $0.33\mathrm{Na_2S} + 0.67\mathrm{GeS_2}$ sample. Upon crystallization, the spectra show striking similarity to the Raman spectra of compounds containing the $Ge_4S_{10}^{4-}$ anion.[59−62] Müller et al. showed that the vibrational fundamentals of the $Ge_4S_{10}^{4-}$ anion could be modeled by T_d symmetry.[59]

$$\Gamma = 3A_1 + 3E + 3T_1 + 6T_2$$

From the T_d character table, it is seen that the A_1, E, and T_2 modes are Raman-active, the T_2 modes are IR-active, while the T_1 modes are neither Raman- nor IR-active. The E modes are expected to have low intensities and to strongly overlap with other modes, leaving only nine expected modes.[59] In the Raman spectrum, the three A_1 modes occur at 463, 348, and 192 cm^{-1}. The presence of these modes in the IR spectrum indicates a breakdown in T_d symmetry. The T_2 modes are centered at 444, 409, 384, 205, and 120 cm^{-1}. Strong similarities exist between the spectra of the glassy and crystallized samples, indicating that discrete $Ge_4S_{10}^{4-}$ anionic groups are present in the glass, in agreement with the findings of Barrau et al.,[41] but the extent of the broadening of the bands, the presence of the shoulder at 390 cm^{-1} in the Raman spectrum, and the intensity of modes in the 300−350 cm^{-1} range of the IR spectrum lead us to believe that branching structures account for the majority of Ge^3 groups in the glass. For clarity, Ge^3 groups that form branching structures will be referred to as Ge^{3B} groups, and Ge^3 groups in $Ge_4S_{10}^{4-}$

dx.doi.org/10.1021/jp4111053 | J. Phys. Chem. B 2014, 118, 1943−1953

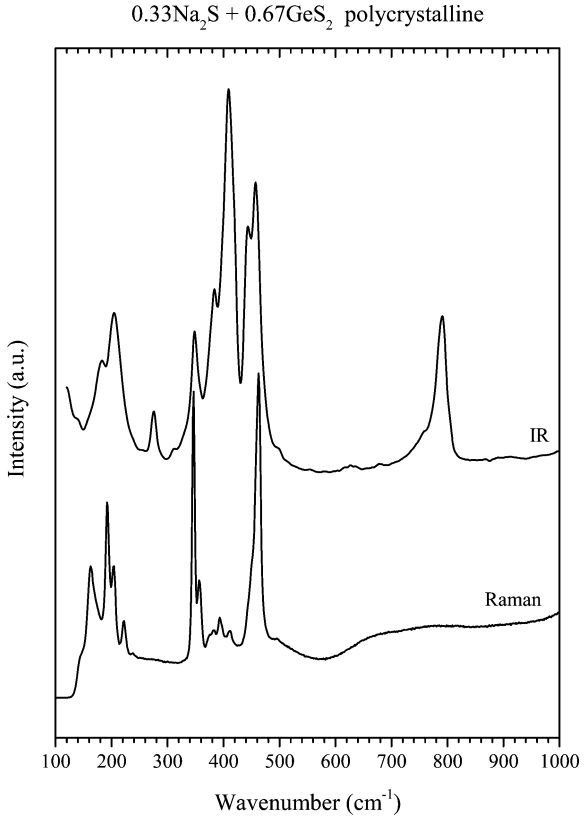

Figure 7. Raman and IR spectra of the polycrystalline $0.33Na_2S + 0.67GeS_2$.

molecular anionic groups will be referred to as Ge^{3M} groups. These structures are shown in Figure 1 for clarity.

At $y = 0.5$, Ge^2, or *meta*-thiogermanate, Na_2GeS_3, structures are formed by further addition of Na_2S and form corner-shared chain structures.[41] The Raman spectrum, Figure 5, has four dominant modes in the range of 300−500 cm^{-1}. The most intense mode at 418 cm^{-1} (415 cm^{-1} in the IR spectrum) is due to stretching of the NBS. The next most intense mode at ∼335 cm^{-1} (shoulder in the IR spectrum) is due to the stretching mode of the BS. The remaining bands centered at 447 and 380 cm^{-1} are likely due to modes arising from a combination of structural groups. The mode at 447 cm^{-1}, which corresponds to the most dominant mode in the IR spectrum, may indicate dimeric edge-sharing Ge^2 groups, $Na_4Ge_2S_6$, that are present in $Na_4Ge_2S_6{\cdot}14H_2O$[63] or possibly Ge^{3B} and Ge^{3M} groups. The relatively strong absorbance in the IR spectrum, Figure 6, at 380 cm^{-1} is consistent with BS modes in GeS_2, and its greater intensity in the $y = 0.5$ composition than that for the $y = 0.6$ composition indicates that the mode is due more to Ge^2 groups, the expected SRO at the $y = 0.5$ composition. The most dominant mode in the Raman spectrum of the $y = 0.6$ glass is at 392 cm^{-1}, and its proximity to the mode at 380 cm^{-1} cannot be ignored. For these reasons, we conclude that both Ge^2 and Ge^1 groups likely contribute to the band at 380 cm^{-1} in the vibrational spectra.

The $y = 0.6$ glass corresponds to the pyro-thiogermanate group, Ge^1, $Na_6Ge_2S_7$; see Figure 1. Two dominant Raman modes are evident in the Raman spectra (Figure 5) at 392 cm^{-1} due to terminal sulfurs and 332 cm^{-1} due to BSs, both of which correspond to shoulders in the IR spectrum at 390 and 330 cm^{-1} (Figure 6). While the IR mode centered at 417 cm^{-1} is assigned to terminal sulfurs, the band centered at 360 cm^{-1} is likely due to BS but cannot be unambiguously assigned to the Ge^1 group because this feature is present in the $y = 0.33$ and 0.5 glasses as well. This mode compares reasonably well with the most intense Raman band of the $Ge_2S_6^{4-}$ anion, which has two edge-shared Ge^2 groups,[63] and it also corresponds to the most dominant Raman band present in α-GeS_2.[57] For these reasons, we tentatively assign this band to edge-sharing Ge^2 species.

Further addition of Na^+ leads to the formation of Ge^0 groups that correspond to the composition $y = 0.67$, Na_4GeS_4 glass. This composition was not reported to be glass-forming by Barrau et al.,[41] where the glasses were prepared in sealed quartz ampules and quenched to room temperature. However, the higher quench rate achieved in the current study, estimated to be $>10^4$ °C/s, was sufficient to bypass crystallization of the Na_4GeS_4 phase. As may be expected, the Raman and IR spectra of the glass indicate a highly symmetric structure, consistent with a completely depolymerized GeS_4^{4-} tetrahedral anion. The most intense Raman band centered at 371 cm^{-1} in Figure 5 is due to the symmetric stretching of the Ge^0 tetrahedron.[64] A shoulder near 391 cm^{-1} shows a strong correlation with the symmetric stretching of the Ge^1 group and with the most intense IR band (also centered at 391 cm^{-1}; see Figure 6). In the IR spectrum, Figure 6, the mode at 391 cm^{-1} is assigned to the asymmetric stretching of the G^0 group, while the high-frequency shoulder of this peak is further evidence of the presence of Ge^1 minority species, presumably formed by minor disproportionation reactions, such as

$$2Ge^0 \rightarrow 2Ge^1 + Na_2S$$

The vibrational spectra of the $yNa_2S + (1-y)GeS_2$ glasses in Figures 5 and 6 exhibit systematic shifts of the bands associated with terminal NBS groups that indicate a depolymerization of GeS_x species. The Ge^n structures present in the glasses are predominantly corner-shared with a minority of edge-shared species. The variety of intermediate-range order (IRO), how SRO structures are connected, leads to broad bands in the vibrational spectra, and in turn, it is believed that it is this structural complexity that leads to a large composition range for homogeneous glass formation that includes the fully depolymerized Ge^0 group. Glass formation of these so-called "ortho" groups is rare unless high-speed roller quenching (or similar) is used, and a notable example includes another sodium *ortho*-salt, sodium *ortho*-borate, Na_3BO_3.[65]

3.4. Ternary MGF Sodium Thiogermanophosphate Glasses, $0.5Na_2S + 0.5[xGeS_2 + (1-x)PS_{5/2}]$. As $PS_{5/2}$ is substituted by GeS_2, with increasing x, in the ternary glasses in the composition range $0.1 \leq x \leq 0.5$, the mode centered at 402 cm^{-1} in the Raman spectra, shown in Figure 8, due to P^1 structures abruptly decreases in intensity as the intensity of a mode centered at 418 cm^{-1} grows rapidly. Assignment of the mode centered at 418 cm^{-1} is ambiguous because it shows strong correlations to both P^0 and Ge^2 groups. The emergence of a mode at 343 cm^{-1} in the $x = 0.1$ spectrum is typical of modes assignable to the symmetric stretching of Ge^4 groups. This mode gradually shifts to 339 cm^{-1} in the $x = 0.4$ glass spectrum, showing strong correlation with Ge^3 groups. Another trend occurs in the spectral region between 450 and 500 cm^{-1}. In the spectrum of the $x = 0$ glass, the mode centered at 480 cm^{-1}, due to S−S bonds, shifts to 490 cm^{-1} with the growth of a new mode at ∼460 cm^{-1}. In the spectrum of the $x = 0.4$ glass, this mode is centered at 463 cm^{-1}, which indicates that Ge^3 groups in $Ge_4S_{10}^{4-}$ molecular anions are present in the glass.

dx.doi.org/10.1021/jp4111053 | J. Phys. Chem. B 2014, 118, 1943−1953

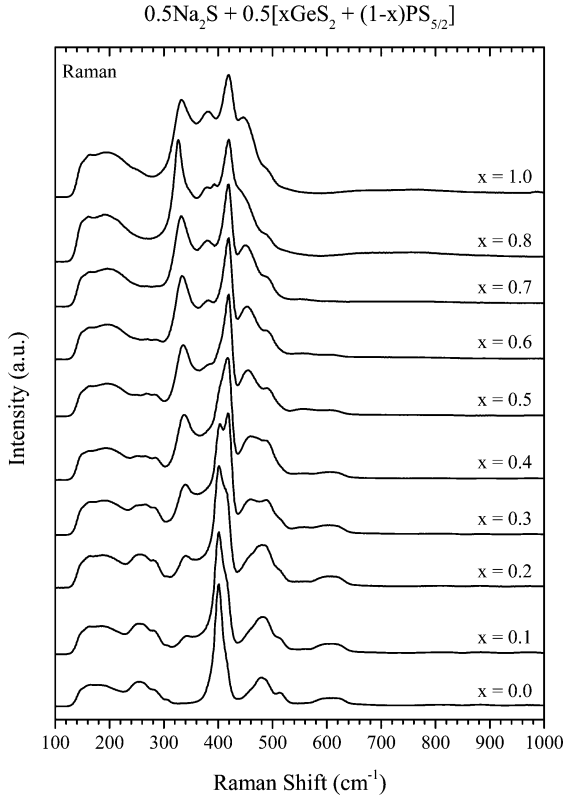

Figure 8. Composition dependence of the Raman spectra of the $0.5Na_2S + 0.5[xGeS_2 + (1-x)PS_{5/2}]$ glasses.

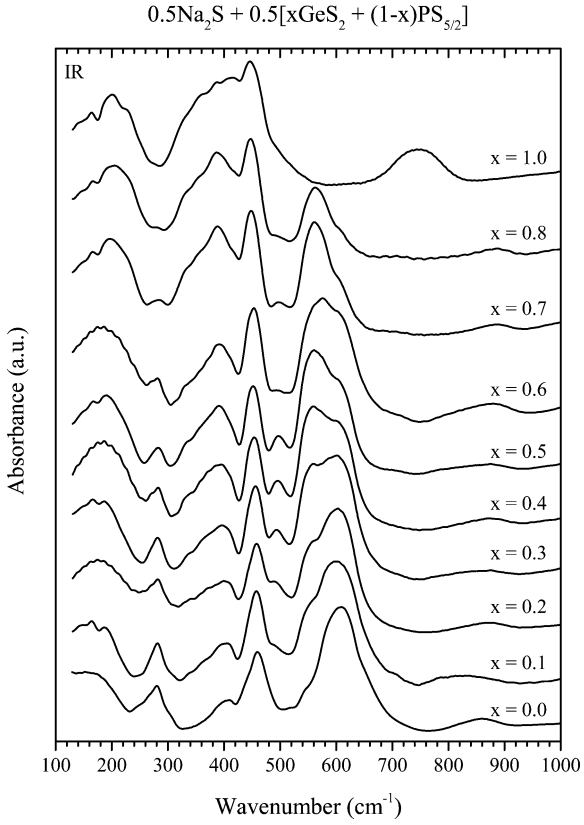

Figure 9. Composition dependence of the IR spectra of the $0.5Na_2S + 0.5[xGeS_2 + (1-x)PS_{5/2}]$ glasses.

Spectral features occurring at wavenumbers above 700 cm^{-1} in the Raman (Figure 8) and IR (Figure 9) spectra of the ternary glasses are due to (nearly unavoidable) advantageous oxide contamination. Integration of the ^{31}P NMR signal indicates that replacement of sulfur by oxygen is less than 2% for all glass samples.

The composition dependence of the IR spectra of the ternary glasses, shown in Figure 9, for $0.1 \leq x \leq 0.5$ glasses are dominated by the reduction in the intensity of the 609 cm^{-1} mode due to asymmetric stretching of the P^1 group, which is coupled with the growth of the 560 cm^{-1} mode due to the P^0 group. Further, the 609 cm^{-1} mode shifts to lower frequency, to ~600 cm^{-1} in the $x = 0.5$ glass, which may indicate P^1 groups linked to Ge^n groups. A mode at 583 cm^{-1}, clearly present in the $x = 0.3$ glass, is due to P^{1P} groups. The growth of a broad mode at ~390 cm^{-1} is assigned to BS in Ge^n groups.

In the $0.1 \leq x \leq 0.5$ composition range, the vibrational spectra indicate that as GeS_2 is exchanged for $PS_{5/2}$, phosphorus groups become more depolymerized, that is, they acquire more Na^+ through the formation of terminal NBS units. In doing so, the phosphorus gains a disproportionate share of the Na^+ charge, $f_{Na(P)} > 0.5(1 - x)$. More specifically, in this process, P^1 groups are converted to P^0 groups. The evidence of Ge^4 and Ge^3 groups in these glasses is consistent with this trend, that is, for the phosphorus groups to gain Na^+, the germanium groups must lose Na^+. The ^{31}P MAS NMR spectra allow discrimination between these sites, as seen in Figure 10. The diminishing of the 94 ppm resonance due to P^1 and the increased intensity of the 83 ppm resonance due to P^0 confirm that P^1 groups are being converted to P^0 groups. The P^1 companion, P^{1P}, resonance at 100−105 ppm seems to be more stable in the presence of Ge^n species. The modest change in isotropic

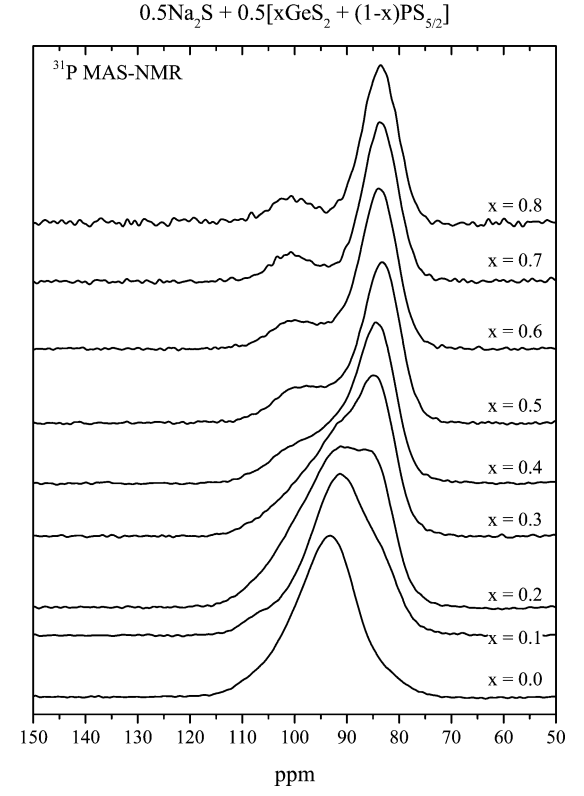

Figure 10. Composition dependence of the ^{31}P MAS NMR spectra of the $0.5Na_2S + 0.5[xGeS_2 + (1-x)PS_{5/2}]$ glasses.

dx.doi.org/10.1021/jp4111053 | J. Phys. Chem. B 2014, 118, 1943−1953

chemical shift of both the P^1 and P^{1P} resonances in this composition range may indicate bonding with Ge^n groups; however, slight changes in the geometry of the phosphorus tetrahedra could also account for the change in chemical shift.

The substitution of $PS_{5/2}$ by GeS_2, increasing x, leads to a distinct narrowing of the band due to symmetric stretching of BS at ~330 cm^{-1} in the Raman spectrum of the x = 0.8 glass shown in Figure 8. Further, the frequency of this mode at 326 cm^{-1} correlates well with Ge^2 chains in crystalline samples. The emergence of the mode centered at 393 cm^{-1} is likely due to the deformation of BS in Ge^3 groups that form $Ge_4S_{10}^{4-}$ molecular anions. If Ge^2 structures donate Na^+ to P^1 groups, P^0 isolated tetrahedra and Ge^3 species are formed. This gives rise to $Ge_4S_{10}^{4-}$, and potentially, the shorter Ge^2 chains may be able to assume local coordination that is similar to that of crystalline Na_2GeS_3. The Raman spectra (Figure 8) of the glasses at x = 0.6 and 0.7 do not exhibit the same band narrowing as the spectrum for the x = 0.8 glass. This is likely due to the increased $PS_{5/2}$ content. As more Ge^2 groups are converted to Ge^3 groups, Ge^3 groups exist in sufficient quantities to form branching networks, Ge^{3B}, rather than molecular anions, Ge^{3M}. The IR spectra (Figure 9) in this composition range also indicate a depolymerization of phosphorus structures, $P^1 \rightarrow P^0$, as the 609 cm^{-1} mode intensity decreases with x, while the 560 cm^{-1} mode increases with x. IR bands centered near 450 and 390 cm^{-1} are consistent with a mixture of Ge^2 and Ge^3 species.

The ^{31}P MAS NMR spectra of the glasses for $0.6 \leq x \leq 0.8$ are dominated by two resonances at 83 and 100 ppm. The 83 ppm resonance is due to P^0 groups, and the resonance at 100 ppm is due to P^{1P} groups. The chemical shift of the P^{1P} peak is shifted a few ppm from its 105 ppm chemical shift in the x = 0 glass. As stated previously, the change in chemical shift may be due to P^{1P} bound to Ge^n groups, but slight changes in geometry of the P^{1P} group may also account for this change.

The Raman, IR, and ^{31}P MAS NMR structural studies of the $0.5Na_2S + 0.5[xGeS_2 + (1-x)PS_{5/2}]$ glasses provide evidence that when the sodium pyro-thiophosphate glass is reacted with the sodium *meta*-thiogermanate glass, phosphorus structures are depolymerized, and germanium structures are polymerized. This implies the following disproportion reaction.

$$P^1 + Ge^2 \rightarrow P^0 + Ge^3$$

A possible reason for this reaction is due to resonance stabilization of the phosphorus species, where the extra valence electron nominally associated with the phosphorus−sulfur double bond is spread over two P−S bonds in the P^2 group, three P−S bonds in the P^1 group, and four bonds in the P^0 group. In this way, we would expect that the energy of the P^1 group moves to a lower, more stable energy than the P^2 group, and the energy of the P^0 group moves to a lower, more stable energy than the P^1 group. According to Blachnik and Rabe, P_4S_{10} and $Ge_4S_{10}^{4-}$ are isostructural; therefore, they attempted to form mixed anionic cages of $Ge_{4-x}P_xS_{10}^{(4-x)-}$ by annealing mixtures of P_4S_{10} and $Ge_4S_{10}^{4-}$.[44] While the attempts were unsuccessful, they were able to construct a partial phase diagram using DTA and DSC measurements. Interestingly, the results show unequal sharing of the Na^+ ion, in which the Ge^3 groups are polymerized to form Ge^4, and the P^3 groups are depolymerized, consistent with our results found here. The Ge-rich compositions disproportionate to P^0 groups, whereas the P-rich compositions form P^2 groups due to low Na^+ ion concentration. Further, P^1 groups were not found to be formed, perhaps because it is a peritectic phase; this suggests that it is a thermodynamically less stable phase.

From the SRO analysis of the Raman, IR, and NMR spectroscopy results described above, it is possible to develop a structural model of the $0.5Na_2S + 0.5[xGeS_2 + (1-x)PS_{5/2}]$ glasses. Phosphorus populations were determined by integration of the NMR spectra. Germanium populations were determined through charge neutrality considerations. The model that is presented as a compositional map of all of the various germanium and phosphorus SRO structural groups is shown in Figure 11.

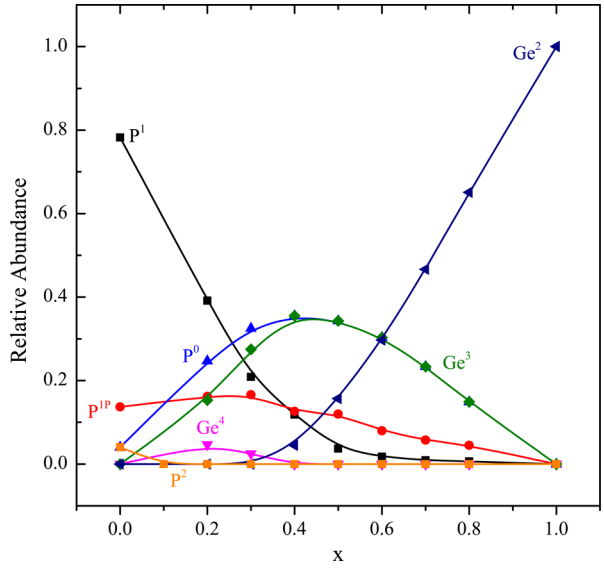

Figure 11. Fraction of the structural units in the $0.5Na_2S + 0.5[xGeS_2 + (1-x)PS_{5/2}]$ glasses as determined by ^{31}P MAS NMR for phosphorus species. Germanium species are calculated from the remaining charge determined from ^{31}P MAS NMR while maintaining charge balance.

The unequal sharing of Na^+ by the phosphorus structural groups caused by the addition of GeS_2 leads to a decrease in the fraction of the P^1 groups and an increase in the fraction of the P^0 groups. The small fraction of P^2 groups in the x = 0 glass, nominally $Na_2PS_{7/2}$, is immediately depolymerized upon addition of Na_2Ge_3, and thus, the P^2 group is not present in any of MGF glasses. The P^{1P} group appears to be more stable than the P^1 group in the presence of Ge^n species; therefore, its concentration is roughly constant for $0.0 \leq x \leq 0.3$. For $x > 0.3$, the Ge^n concentration is large enough to enable the conversion of P^{1P} groups to P^0 groups, consistent with the preference of phosphorus to be overly modified in these glasses, that is, as described above, for the phosphorus structural groups to possess more Na^+ NBS structures than expected from the composition, namely, $f_{Na(P)} > 0.5(1 - x)$.

The germanium populations were determined from the requirement of charge neutrality and the phosphorus SRO structural units determined by ^{31}P MAS NMR, and both show excellent agreement with analysis of the vibrational spectra. For example, the x = 0.4 glass has the maximum Ge^3 population from the model, and the Raman modes at 338 and 463 cm^{-1}, in addition to the IR mode at 454 cm^{-1}, match the modes of the $0.33Na_2S + 0.67GeS_2$ glass.

dx.doi.org/10.1021/jp4111053 | J. Phys. Chem. B 2014, 118, 1943−1953

4. CONCLUSIONS

The yNa$_2$S + (1−y)GeS$_2$ and yNa$_2$S + (1−y)PS$_{5/2}$ glasses were synthesized and their structures characterized by IR, Raman, and ^{31}P MAS NMR. The mixing of a sodium pyrothiophosphate glass, Na$_2$PS$_{7/2}$, with a sodium *meta*-thiogermanate glass, Na$_2$GeS$_3$, leads to unequal sharing of the Na$^+$ toward the phosphorus to create more depolymerized phosphorus SRO structures where $f_{Na(P)}$, the fraction of Na associated with the phosphorus SRO structures, in the glass is always greater than 0.5(1 − x), that expected from equal sharing of the Na$^+$. The Ge SRO structures in these MGF glasses exhibit a tendency to form discrete, molecular anionic structures, such as Na$_4$Ge$_4$S$_{10}$. In all MGF compositions, phosphorus groups are associated with a disproportionately large number of Na$^+$, while germanium groups are Na$^+$-deficient. A structural model based on SRO structures in the glasses was developed that shows the precise composition dependence of all SRO structures in these glasses. This model has at least two important results. First, it explicitly gives the fractions of all BS and NBS structures in the glass and can be used to analyze properties such as the T_g that depend in part on the relatively fractions of BS and NBS in glass. Second, this model also explicitly gives the fractions of all SRO groups that possess charge-compensating Na$^+$ cations. As such, it can be used to analyze properties such as the Na$^+$ ion conductivity that is highly dependent on the local, hence anionic, environments of the Na$^+$ ions. In future publications in this series, we will use this model to describe these and other properties in this way.

AUTHOR INFORMATION

Corresponding Author

†E-mail: swmartin@iastate.edu. Phone: 515-294-0745.

Present Address

[†]C.B.: Missouri University of Science and Technology, Rolla, MO, 65409.

Notes

The authors declare no competing financial interest.

ACKNOWLEDGMENTS

This research was supported by the National Science Foundation under Grant Number DMR-0710564, and this research support is gratefully acknowledged. The authors would also like to acknowledge the help of the ISU Chemistry Department Chemical Services Laboratory where the NMR measurements were made and to thank spectroscopist Dr. Sarah Cady in particular for her help in conducting the ^{31}P MAS NMR measurements of these glasses.

REFERENCES

(1) Crabtree, G. W.; Lewis, N. S. Solar Energy Conversion. *Phys. Today* **2007**, *60*, 37−42.

(2) Whitesides, G. M.; Crabtree, G. W. Don't Forget Long-Term Fundamental Research in Energy. *Science* **2007**, *315*, 796−798.

(3) Abruna, H. D.; Kiya, Y.; Henderson, J. C. Batteries and Electrochemical Capacitors. *Phys. Today* **2008**, *61*, 43−47.

(4) Whittingham, M. S. Materials Challenges Facing Electrical Energy Storage. *MRS Bull.* **2008**, *33*, 411−419.

(5) Wray, P. Lithium Lowdown. *Am. Ceram. Soc. Bull.* **2009**, *88*, 17−24.

(6) Goodenough, J. B.; Kim, Y. Challenges for Rechargeable Li Batteries. *Chem. Mater.* **2010**, *22*, 587−603.

(7) Burckhardt, W.; Rudolph, B. Ion Conducting Glasses — Potential Solid Electrolytes for All-Solid Batteries. *Silikattechnik* **1991**, *42*, 275−278.

(8) Martin, S. W. Ionic Conduction in Phosphate Glasses. *J. Am. Ceram. Soc.* **1991**, *74*, 1767−1784.

(9) Pradel, A.; Kuwata, N.; Ribes, M. Ion Transport and Structure in Chalcogenide Glasses. *J. Phys.: Condens. Matter* **2003**, *15*, S1561−S1571.

(10) Rao, K. J.; Ganguli, M. Lithium Ion Conducting Glasses. *Handb. Solid State Batteries Capacitors* **1995**, 189−208.

(11) Kim, Y.; Saienga, J.; Martin, S. W. Preparation and Characterization of Germanium Oxy-Sulfide GeS$_2$−GeO$_2$ Glasses. *J. Non-Cryst. Solids* **2005**, *351*, 1973−1979.

(12) Kim, Y.; Saienga, J.; Martin, S. W. Anomalous Ionic Conductivity Increase in Li$_2$S + GeS$_2$ + GeO$_2$ Glasses. *J. Phys. Chem. B* **2006**, *110*, 16318−16325.

(13) Pradel, A.; Rau, C.; Bittencourt, D.; Armand, P.; Philippot, E.; Ribes, M. Mixed Glass Former Effect in the System 0.3Li$_2$S − 0.7[(1−x)SiS$_2$ − xGeS$_2$]: A Structural Explanation. *Chem. Mater.* **1998**, *10*, 2162−2166.

(14) Schuch, M.; Mueller, C. R.; Maass, P.; Martin, S. W. Mixed Barrier Model for the Mixed Glass Former Effect in Ion Conducting Glasses. *Phys. Rev. Lett.* **2009**, *102*, 145902/1−145902/4.

(15) Anantha, P. S.; Hariharan, K. Structure and Ionic Transport Studies of Sodium Borophosphate Glassy System. *Mater. Chem. Phys.* **2005**, *89*, 428−437.

(16) Tsuchiya, T.; Moriya, T. Anomalous Behavior of Physical and Electrical Properties in Borophosphate Glasses Containing R$_2$O and V$_2$O$_5$. *J. Non-Cryst. Solids* **1980**, *38*−*39*, 323−328.

(17) Zielniok, D.; Cramer, C.; Eckert, H. Structure/Property Correlations in Ion-Conducting Mixed-Network Former Glasses: Solid-State NMR Studies of the System Na$_2$O−B$_2$O$_3$−P$_2$O$_5$. *Chem. Mater.* **2007**, *19*, 3162−3170.

(18) Christensen, R.; Byer, J.; Olson, G.; Martin, S. W.; Shu, X. Mixed Glass-Former Effect in Sodium Borophosphate Glass. *Am. Ceram. Soc. Bull.* **2011**, *90*, 19−22.

(19) Seo, I.; Martin, S. W. Preparation and Characterization of Fast Ion Conducting Lithium Thio-Germanate Thin Films Grown by RF Magnetron Sputtering. *J. Electrochem. Soc.* **2011**, *158*, A465−A470.

(20) Yao, W.; Martin, S. W. Ionic Conductivity of Glasses in the MI + M$_2$S + (0.1Ga$_2$S$_3$ + 0.9GeS$_2$) System (M = Li, Na, K and Cs). *Solid State Ionics* **2008**, *178*, 1777−1784.

(21) Saienga, J.; Martin, S. W. The Comparative Structure, Properties, and Ionic Conductivity of LiI + Li$_2$S + GeS$_2$ Glasses Doped with Ga$_2$S$_3$ and La$_2$S$_3$. *J. Non-Cryst. Solids* **2008**, *354*, 1475−1486.

(22) Kim, Y.; Martin, S. W. Ionic Conductivities of Various GeS$_2$-Based Oxy-Sulfide Amorphous Materials Prepared by Melt-Quenching and Mechanical Milling Methods. *Solid State Ionics* **2006**, *177*, 2881−2887.

(23) Fusco, F. A.; Tuller, H. L. Fast Ion Transport in Glasses. *Superionic Solids Solid Electrolytes: Recent Trends* **1989**, 43−110.

(24) Tuller, H. L.; Barsoum, M. W. Glass Solid Electrolytes: Past, Present and Near Future — The Year 2004. *J. Non-Cryst. Solids* **1985**, *73*, 331−350.

(25) Robert, G.; Malugani, J. P.; Saida, A. Fast Ionic Silver and Lithium Conduction in Glasses. *Solid State Ionics* **1981**, *3*−*4*, 311−315.

(26) Malugani, J. P.; Robert, G. Ionic Conductivity in the Glasses LiPO$_3$−LiX (X = I, Br, Cl). *Mater. Res. Bull.* **1979**, *14*, 1075−1081.

(27) Hayashi, A.; Noi, K.; Sakuda, A.; Tatsumisago, M. Superionic Glass-Ceramic Electrolytes for Room-Temperature Rechargeable Sodium Batteries. *Nat Commun.* **2012**, *3*, 856.

(28) Hayashi, A.; Yamashita, H.; Tatsumisago, M.; Minami, T. Characterization of Li$_2$S−SiS$_2$−Li$_x$MO$_y$ (M=Si, P, Ge) Amorphous Solid Electrolytes Prepared by Melt-Quenching and Mechanical Milling. *Solid State Ionics* **2002**, *148*, 381−389.

(29) Minami, T.; Hayashi, A.; Tatsumisago, M. Recent Progress of Glass and Glass-Ceramics as Solid Electrolytes for Lithium Secondary Batteries. *Solid State Ionics* **2006**, *177*, 2715−2720.

(30) Tatsumisago, M.; Hayashi, A. Superionic Glasses and Glass-Ceramics in the Li_2S–P_2S_5 System for All-Solid-State Lithium Secondary Batteries. *Solid State Ionics* **2012**, *225*, 342–345.
(31) Hayashi, A.; Morishima, H.; Tadanaga, K.; Tatsumisago, M. Characterization of Solid Electrolytes Prepared from Ionic Glass and Ionic Liquid for All-Solid-State Lithium Batteries. *Solid State Ionics* **2011**, *192*, 126–129.
(32) Tatsumisago, M.; Hayashi, A. All-Solid-State Lithium Secondary Batteries Using Sulfide-Based Glass Ceramic Electrolytes. *Funct. Mater. Lett.* **2008**, *1*, 31–36.
(33) Storek, M.; Boehmer, R.; Martin, S. W.; Larink, D.; Eckert, H. NMR and Conductivity Studies of the Mixed Glass Former Effect in Lithium Borophosphate Glasses. *J. Chem. Phys.* **2012**, *137*, 124507/1–124507/12.
(34) Brow, R. K.; Tallant, D. R.; Hudgens, J. J.; Martin, S. W.; Irwin, A. D. The Short-Range Structure of Sodium Ultraphosphate Glasses. *J. Non-Cryst. Solids* **1994**, *177*, 221–228.
(35) Martin, S. W. Review of the Structures of Phosphate Glasses. *Eur. J. Solid State Inorg. Chem.* **1991**, *2*, 163–205.
(36) Potrzebowski, M. J.; Kazmierski, S.; Kassassir, H.; Miksa, B. Phosphorus-31 NMR Spectroscopy of Condensed Matter. *Annu. Rep. NMR Spectrosc.* **2010**, *70*, 35–114.
(37) Jager, C.; Hartmann, P.; Witter, R.; Braun, M. New 2D NMR Experiments for Determining the Structure of Phosphate Glasses: A Review. *J. Non-Cryst. Solids* **2000**, *263&264*, 61–72.
(38) Mutolo, P. F.; Witschas, M.; Regelsky, G.; Schmedt auf der Guenne, J.; Eckert, H. Nuclear Magnetic Resonance (NMR) Studies of the Local Structure of Phosphorus Chalcogenide Glasses: An Overview. *J. Non-Cryst. Solids.* **1999**, *256&257*, 63–72.
(39) Ribes, M.; Barrau, B.; Souquet, J. L. Sulfide Glasses: Glass Forming Region, Structure and Ionic Conduction of Glasses in Na_2S–XS_2 (X = Si; Ge), Na_2S–P_2S_5 and Li_2S–GeS_2 System. *J. Non-Cryst. Solids* **1980**, *38–39*, 271–276.
(40) Barrau, B.; Kone, A.; Ribes, M.; Souquet, J. L.; Maurin, M. Synthesis and Study of the Electrical Conductivity of Glasses Belonging to the Sodium Monosulfide-Germanium Disulfide System. *C. R. Hebd. Seances Acad. Sci., Ser. C* **1978**, *287*, 43–46.
(41) Barrau, B.; Ribes, M.; Maurin, M.; Kone, A.; Souquet, J. L. Glass Formation, Structure and Ionic Conduction in the Sodium Sulfide–Germanium Sulfide (Na_2S–GeS_2) System. *J. Non-Cryst. Solids* **1980**, *37*, 1–14.
(42) Ribes, M.; Ravaine, D.; Souquet, J. L.; Maurin, M. Synthese, Structure, et Conduction Ionique De Nouveaux Verres a Base De Sulfures. *Rev. Chim. Miner.* **1979**, *16*, 339–347.
(43) Maier, L.; Vanwazer, J. R. Principles of Phosphorus Chemistry. 13. Thiophosphate Salts and Esters. *J. Am. Chem. Soc.* **1962**, *84*, 3054–3058.
(44) Bischoff, C.; Schuller, K.; Haynes, M.; Martin, S. W. Structural Investigations of $y$$Na_2S$ + $(1-y)PS_{5/2}$ Glasses Using Raman and Infrared Spectroscopies. *J. Non-Cryst. Solids* **2012**, *358*, 3216–3222.
(45) Zhou, Z. H.; Kamiya, K.; Tsutsumi, K.; Hashimoto, T.; Nasu, H. Structure of Na_2S–GeS_2 Sulphide Glasses — Comparison with Na_2O–GeO_2 Oxide Glasses. *Phys. Chem. Glasses* **1999**, *40*, 146–152.
(46) Blachnik, R.; Rabe, U. Thermal Behavior of the Mixtures Na_2S–P_4S_{10} and $Na_4Ge_4S_{10}$–P_4S_{10} of the System Na_2S–GeS_2-P_4S_{10}. *Z. Anorg. Allg. Chem.* **1980**, *462*, 199–206.
(47) Larink, D.; Ren, J.; Eckert, H. Spectral Editing Based on Scalar Spin–Spin Interactions: New Results on the Structure of Meta-thiophosphate Glasses. *Solid State Nucl. Magn. Reson.* **2012**, *45–46*, 30–35.
(48) Brown, S. P.; Perez-Torralba, M.; Sanz, D.; Claramunt, R. M.; Emsley, L. Determining Hydrogen-Bond Strengths in the Solid State by NMR: The Quantitative Measurement of Homonuclear J Couplings. *Chem. Comm.* **2002**, *0*, 1852–1853.
(49) Fayon, F.; King, I. J.; Harris, R. K.; Evans, J. S. O.; Massiot, D. Application of the Through-Bond Correlation NMR Experiment to the Characterization of Crystalline and Disordered Phosphates. *C. R. Chim.* **2004**, *7*, 351–361.
(50) Gjikaj, M.; Brockner, W.; Adam, A. Stabilization of Highly Reactive "Naked Anions": Synthesis, Crystal Structure and Vibrational Spectrum of $[Na(12\text{-Crown-}4)_2]_2$ $[P_2S_6]\cdot CH_3CN$. *Z. Anorg. Allg. Chem.* **2006**, *632*, 279–283.
(51) Queignec, M.; Evain, M.; Brec, R.; Sourisseau, C. Vibrational Study of Some Low-Dimensional Niobium–Phosphorus-Sulfide Compounds, P_2NbS_8, PNb_2S_{10}, and $P_2Nb_4S_{21}$. *J. Solid State Chem.* **1986**, *63*, 89–109.
(52) Tranquille, M.; Fouassier, M. Vibrational Spectra of Matrix Isolated Al_2Cl_6. Isotopic Fine Structure and Valence Force Field. *J. Chem. Soc., Faraday Trans 2* **1980**, *76*, 26–41.
(53) Eckert, H.; Zhang, Z.; Kennedy, J. H. Structural Transformation of Non-Oxide Chalcogenide Glasses. The Short-Range Order of Lithium Sulfide (Li_2S)–Phosphorus Pentasulfide (P_2S_5) Glasses Studied by Quantitative Phosphorus-31, Lithium-6, and Lithium-7 High-Resolution Solid-State NMR. *Chem. Mater.* **1990**, *2*, 273–279.
(54) Minami, K.; Hayashi, A.; Tatsumisago, M. Crystallization Process for Superionic $Li_7P_3S_{11}$ Glass-Ceramic Electrolytes. *J. Am. Ceram. Soc.* **2011**, *94*, 1779–1783.
(55) Minami, K.; Hayashi, A.; Tatsumisago, M. Preparation and Characterization of Superionic Conducting $Li_7P_3S_{11}$ Crystal from Glassy Liquids. *J. Ceram. Soc. Jpn.* **2010**, *118*, 305–308.
(56) Brinkmann, C.; Eckert, H.; Wilmer, D.; Vogel, M.; Schmedt auf der Guenne, J.; Hoffbauer, W.; Rau, F.; Pfitzner, A. Re-Entrant Phase Transition of the Crystalline Ion Conductor $Ag_7P_3S_{11}$. *Solid State Sci.* **2004**, *6*, 1077–1088.
(57) Cernosek, Z.; Cernoskova, E.; Benes, L. Raman Scattering in GeS_2 Glass and Its Crystalline Polymorphs Compared. *J. Mol. Struct.* **1997**, *435*, 193–198.
(58) Kamitsos, E. I.; Kapoutsis, J. A.; Chryssikos, G. D.; Taillades, G.; Pradel, A.; Ribes, M. Structure and Optical Conductivity of Silver Thiogermanate Glasses. *J. Solid State Chem.* **1994**, *112*, 255–261.
(59) Müller, A.; Cyvin, B. N.; Cyvin, S. J.; Pohl, S.; Krebs, B. Spectroscopic Studies of As_4O_6, Sb_4O_6, P_4S_{10}, $Ge_4S_{10}^{4-}$ and Organometallic Compounds Containing the M_4X_6 Cage. The Raman and I.R. Spectrum of $Ge_4S_{10}^{4-}$. *Spectrochimica Acta, Part A* **1976**, *32*, 67–74.
(60) Ribes, M.; Olivier-Fourcade, J.; Philippot, E.; Maurin, M. Etude Structurale de Thiocomposés À Groupement Anionique de Type Tétrane $Na_4X_4S_{10}$ (X = Ge, Si) Et $Ba_2Ge_4S_{10}$. *J. Solid State Chem.* **1973**, *8*, 195–205.
(61) Rangan, K. K.; Kanatzidis, M. G. Mesolamellar Thiogermanates $[C_nH_{2n+1}nH_3]_4Ge_4S_{10}$. *Inorg. Chim. Acta* **2004**, *357*, 4036–4044.
(62) Nelson, C. R.; Poling, S. A.; Martin, S. W. Synthesis and Characterization of Potassium, Rubidium, and Cesium Thiogermanate Glasses. *J. Non-Cryst. Solids* **2004**, *337*, 78–85.
(63) Krebs, B.; Pohl, S.; Schiwy, W. Darstellung und Struktur von $Na_4Ge_2S_6\cdot 14H_2O$ und $Na_4Sn_2S_6\cdot 14H_2O$. *Z. Anorg. Allg. Chem.* **1972**, *393*, 241–252.
(64) Seo, I.; Martin, S. W. Structural Properties of Lithium Thio-Germanate Thin Film Electrolytes Grown by Radio Frequency Sputtering. *Inorg. Chem.* **2011**, *50*, 2143–2150.
(65) Martin, S. W.; Cooper, E. I.; Angell, C. A. CO_2 Retention in High-Alkali Borate Glasses. *J. Am. Ceram. Soc.* **1983**, *66*, 153–154.